Modelling ground deformations in volcanic areas by using SAR interferograms

G. Nunnari[1], G. Puglisi[2],
F. Guglielmino[2], M. Coltelli[2]

[1]Dipartimento di Ingegneria Elettrica, Elettronica e dei Sistemi
Università di Catania (Italy)
Viale A. Doria, 6, 95125 – Catania, Italy,
Tel. +39 095 7382306, e-mail:gnunnari@dees.unict.it

[2]Istituto Nazionale di Geofisica e Vulcanologia,
Sezione di Catania
Piazza Roma, 3, 95122 – Catania, Italy
Tel. +39 095 716581,e-mail:puglisi-g@ct.ingv.it

Abstract

The inversion problem dealt with is the identification of the parameters of a magma-filled dike which causes observable changes in ground deformation data. It is supposed that ground deformation data are measured by using the SAR (Synthetic Aperture Radar) Interferometry technique. The inversion approach, which is carried out by a systematic search technique based on the Simulated Annealing (SA) optimization algorithm, guarantees a high degree of accuracy. The results given in the paper are supported by experiments carried out using an interactive software tool developed ad hoc, which allows both direct and inverse modeling of SAR interferometric data related to the opening of a crack at the beginning and throughout a volcanic activity episode.

Introduction

SAR interferometry is currently one of the most powerful techniques for observation of the earth's surface in particular for topographical measurement of vast geographical areas [Massonnet and Ribaute, 1993], [Gabriel et. al, 1989],[Curlander and McDonough, 1991], [McCloy, 1995] and small surface changes of a surface over a pre-defined time interval (Differential Radar Interferometry). SAR systems record both amplitude and phase of the back scattered radar echoes. If two SAR images from slightly different viewing angles are considered (interferometric pair) their difference (interferometric fringes) can be usefully exploited to generate Digital Elevation Maps (DEMs), measuring shifts in tectonic plates, movement of glaciers and so on. Recently SAR interferometry was considered also to monitor ground deformation in volcanic active areas [Coltelli et al., 1996], [Lanari et al., 1996], [Briole et al., 1999] SAR interferometry allows to integrate the techniques traditionally considered to measure ground deformations in volcanic areas such as EDM (Electronic Distance Measuring) or GPS (Global Positioning System) techniques.

The inversion problem considered in this paper consists of identifying the geometric and cinematic parameters of a magma-filled dike, which will be indicated as the source, by observing the changes it causes in SAR interferometric images. Analysis of the mathematical model conceived by Okada [Okada, 1985] show that the inversion problem is an extremely nonlinear one. Hence the inversion solution cannot be obtained only in terms of optimisation approaches. In this paper it is shown that in spite of the high degree of non-linearity the inverse problem can be unambiguously solved and an appreciable degree of accuracy can be obtained by using a randomised optimisation algorithms such the Simulated Annealing (SA) algorithm.

Direct Modelling

Generation of SAR synthetic data

The model refers to Mt. Etna volcano (Sicily – Italy), where a number of eruptions have been originated by in dikes opening from a certain depth toward the surface. These phenomena are accompanied by ground deformations and anomalies in the magnetic and gravity fields. The considered geophysical phenomena may be observed when a crack opens up due to the intrusion of magma. Compared to the real situation, the Okada source model, subsequently described, is of course greatly simplified.

The Okada model

This model gives the analytical expression of the surface displacements, strains and tilts due to inclined shear and tensile faults in a half-space. In this section, only the tensile components of the deformations are given, in order to illustrate the level of complexity of the direct model.

Let O(X,Y,Z) be a Cartesian coordinate system representing the traditional UTM system where X and Y represent the East and North directions respectively, while Z represents the vertical direction. Let us consider a dislocation according to the Okada model, having the geometric parameters represented in Fig. 1 whose symbols are described in Tab. I.

Variable	Symbol	Units of Measure	Ranges
Strike	σ	Degrees	[0,360]
Dip	δ	Degrees	[0,90]
Length	L	Meters	[1000,7000]
Width	W	Meters	[1000,5000]
Opening	U3	Meters	[1,5]
Longitude	Xb	Meters	[-10000,10000]
Latitude	Yb	Meters	[-10000,1000]
Depth	Zb	Meters	[-1000,-7000]

Table I Variables, related symbols, unit of measures and ranges considered for the simulation experiments carried out in this paper.

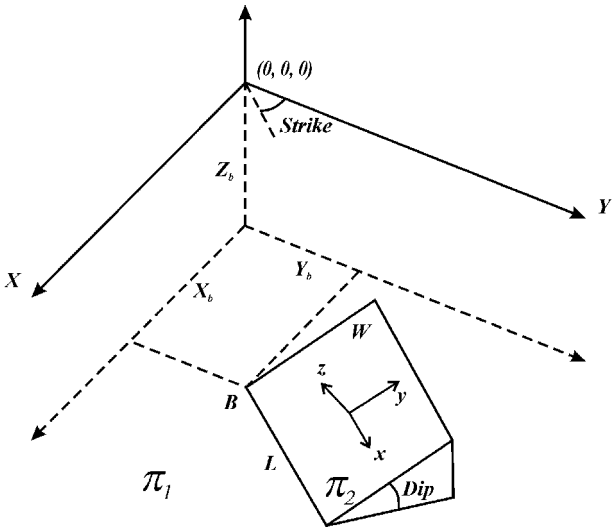

Figure 1 The Okada dislocation Model.

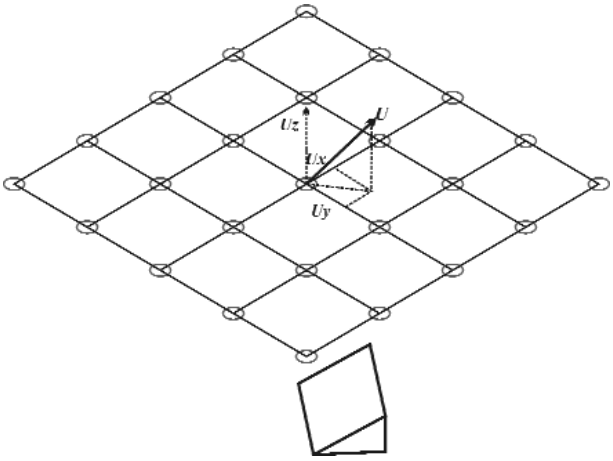

Figure 2 The deformation vector U and its components

The point B, having coordinates (X_B,Y_B,Z_B), lies on the plane π_1, parallel to the plane XY. The side L (Length) of dislocation is supposed to lay on the π_1 plane being the point B one of its vertices, while the side W (Width) is a segment laying on the plane π_2, inclined by an angle referred as Dip with respect to π_1 and orthogonal to L.

Moreover, let us consider a further reference system *o(x,y,z)* having the x, y axis on the π_2 plane and the z axes orthogonal to π_2. In this reference system, x is parallel to L, while y is parallel to W.

The components of the movement caused by a tensile dislocation (tensile fault) relative to a generic point on the plane XY referred to the *o(x,y,z)* system were obtained by Okada, are represented by the following relations (see also Fig. 2).

$$\begin{cases} u_x = \dfrac{U_3}{2\pi}\left[\dfrac{q^2}{R(R+\eta)} - I_3 \sin^2\delta\right] \\ u_y = \dfrac{U_3}{2\pi}\left[\dfrac{-\tilde{d}q}{R(R+\xi)} - \sin\delta\left\{\dfrac{\xi q}{R(R+\eta)} - \tan^{-1}\dfrac{\xi\eta}{qR}\right\} - I_1 \sin^2\delta\right] \\ u_z = \dfrac{U_3}{2\pi}\left[\dfrac{\tilde{y}q}{R(R+\xi)} + \cos\delta\left\{\dfrac{\xi q}{R(R+\eta)} - \tan^{-1}\dfrac{\xi\eta}{qR}\right\} - I_5 \sin^2\delta\right] \end{cases}$$

where

$$\begin{cases} p = y\cos\delta + d\sin\delta \\ q = y\sin\delta - d\cos\delta \\ \tilde{y} = \eta\cos\delta + q\sin\delta \\ \tilde{d} = \eta\sin\delta - q\cos\delta \\ R^2 = \xi^2 + \eta^2 + q^2 = \xi^2 + \tilde{y}^2 + \tilde{d}^2 \\ X^2 = \xi^2 + q^2 \end{cases}$$

being

$$\begin{cases} I_1 = \dfrac{\mu}{\lambda+\mu}\left[\dfrac{-1}{\cos\delta}\dfrac{\xi}{R+\tilde{d}}\right] - \dfrac{\sin\delta}{\cos\delta} I_5 \\ I_2 = \dfrac{\mu}{\lambda+\mu}\left[-\ln(R+\eta)\right] - I_3 \\ I_3 = \dfrac{\mu}{\lambda+\mu}\left[\dfrac{1}{\cos\delta}\dfrac{\tilde{y}}{R+\tilde{d}} - \ln(R+\eta)\right] + \dfrac{\sin\delta}{\cos\delta} I_4 \\ I_4 = \dfrac{\mu}{\lambda+\mu}\dfrac{1}{\cos\delta}\left[\ln(R+\tilde{d}) - \ln(R+\eta)\sin\delta\right] \\ I_5 = \dfrac{\mu}{\lambda+\mu}\dfrac{2}{\cos\delta}\tan^{-1}\dfrac{\eta(X+q\cos\delta)+X(R+X)\sin\delta}{\xi(R+X)\cos\delta} \end{cases}$$

if ,cosδ ≠ 0, and

$$\begin{cases} I_1 = -\dfrac{\mu}{2(\lambda+\mu)}\dfrac{\xi q}{(R+\tilde{d})^2} \\ I_3 = \dfrac{\mu}{2(\lambda+\mu)}\left[\dfrac{\eta}{R+\tilde{d}} + \dfrac{\tilde{y}q}{(R+\tilde{d})^2} - \ln(R+\eta)\right] \\ I_4 = -\dfrac{\mu}{\lambda+\mu}\dfrac{q}{R+\tilde{d}} \\ I_5 = -\dfrac{\mu}{\lambda+\mu}\dfrac{\xi\sin\delta}{R+\tilde{d}} \end{cases}$$

if cosδ = 0.

In these equations, (x, y, z) and (ξ, η, q) are coordinates of appropriate reference systems; R, d and appropriate scalar quantities; the symbol "||" represents Chinnery's notation. The other symbols are explained in Tab. 1. Let us indicate by *Pi* be a generic point on a regular a grid defined in the XY plane as shown in Fig. 2. Moreover, let us indicate with u_x, u_y *e* u_z the components of the deformation referred to the *o(x,y,z)* coordinate system measured at the point Pi due to a tensile dislocation. These components can be easily be referred to the *O(X,Y,Z*) coordinate system according to the following transformation formulas:

$$\begin{cases} U_X = u_x \sin\sigma - u_y \cos\sigma \\ U_Y = u_x \cos\sigma + u_y \sin\sigma \\ U_Z = u_z \end{cases}$$

where σ is the Strike angle.

Then, let $\boldsymbol{U}$ be the deformation vector having U_X, U_Y, and U_Z as components. We need to project this vector along the direction of the satellite view to be able to generate an synthetic interferogram. So, let ρ be the vector of the direction cosines that defines the satellite view angle with respect to the O(X,Y,Z). reference system. Hence the searched projection is

$$U_\rho = \rho \cdot U = \rho_X U_X + \rho_Y U_Y + \rho_Z U_Z$$

The quantity Uρ must be scaled into the interval 0-2π to calculate the traditional fringes that characterise an interferogram, by using the relation

$$\overline{U_\rho} = \frac{2\pi}{\lambda} frac\left(\frac{U_\rho}{\lambda}\right)$$

where λ is the principal wave length emitted by the satellite antenna, that is $28*10^{-3}$ m in the case of ERS-2, and frac() is the fractionary part. Examples of synthetic interferograms are reported in the following figures 3 a) and b).

Inverse Modelling

The Simulated Annealing (SA) algorithm is currently one of the most powerful optimisation techniques available. S. A. has been successfully applied to geophysical inversion problems, e. g. the inversion of seismic waveforms (e. g., [Sen and Stoffa, 1991], [Scherbaum et al., 1994]). It is inspired by the optimization process of crystalline structures during the cooling down of a melt. If the liquid cools down slowly the crystals will develop an (almost) perfect structure corresponding to an (almost) absolute energetic minimum. The structures will become less perfect and thus richer in energy if the cooling is faster. The reason for this resides in the fact that, following concepts of statistical mechanics, the particles may escape a certain energy level with a probability which increases with temperature. Temporary less perfect structures are possible. If the cooling process is slow, particles will have more probability to escape local minima and to approach the global one. In turn, fast cooling will «frozen» the particles at the places just where they are since the probability of escaping a certain energy level becomes low. In our optimization with S. A. the particles of the melt correspond to the models which are fluctuating randomly within a certain model space.

In this study the observation grid is assumed to consist of a mesh of 21x21 stations, spaced at a distance of 1000 m, covering a

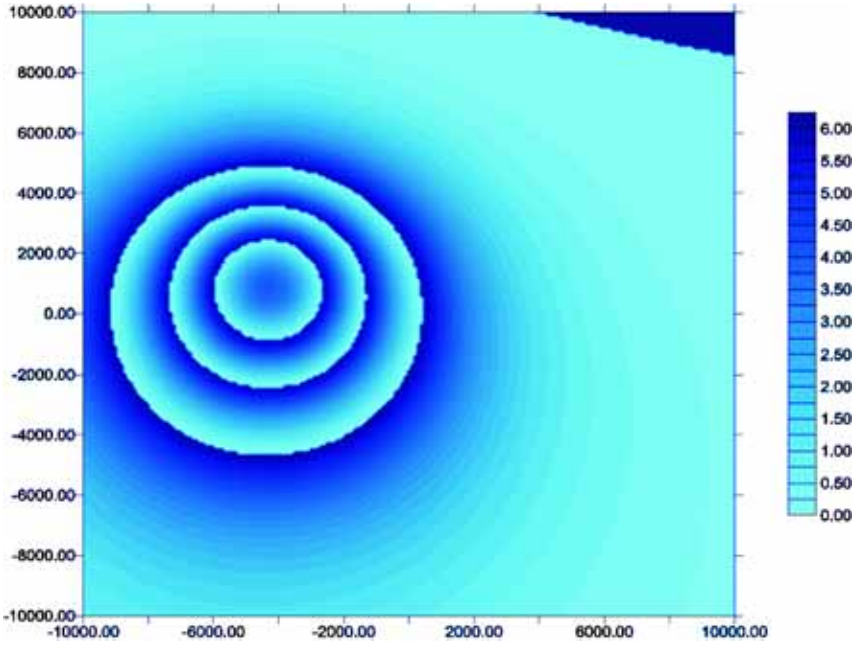

Figure 3a Synthetic interferogram generated by using a tensile dislocation Okada model having the following parameters: Strike = 162°, Dip = 17° Length = 1823m, Width = 1052 m, Opening = 3.82 m, Xb = - 2459 m, Yb=4047 m, Zb = -5361 m.

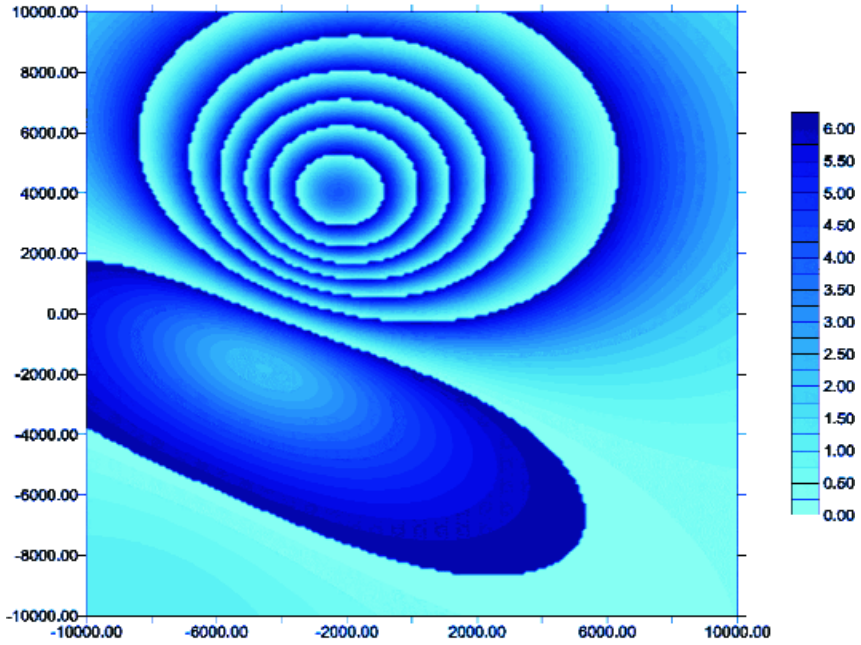

Figure 3b Synthetic interferogram generated by using a tensile dislocation Okada model having the following parameters: Strike = 337°, Dip = 52° Length = 2098 m, Width = 3737 m, Opening = 4.76 m, Xb = - 1612 m, Yb=3729 m, Zb = -4814 m.

region of 20x20 km. The origin of the reference system is assumed to be in the centre of the grid.

The considered cost function Fit is given by the following expression

$$Fit = \frac{1}{N}\sum_{i=1}^{N}\left[\sum_{j=1}^{3}\left|U_R^{(i,j)} - U_C^{(i,j)}\right|\right]$$

where N is the number of points of the grid (i.e. in the considered case N=21x21=441), i is the index of the row position in the grid (i=1..N), j is the direction index (X → j=1, Y → j=2, Z → j=3), UR and UC are the actual and computed deformation respectively.

Several trials were performed in order to

set the free parameters of the SA algorithm. The performance indexes considered to assess the accuracy of the implemented inversion scheme are given by the following relations, where j is the parameter index (j=1..8):

- Mean Error $\boldsymbol{E_M}$

$$E_M^{(j)} = \frac{1}{M}\sum_{i=1}^{M}\left[V_R^{(i,j)} - V_C^{(i,j)}\right]$$

where $V_R^{(i,j)}$ is the generic jth variable of the ith real model, $V_C^{(i,j)}$ is the corresponding calculated variable and M is the number of models ($M=300$).

- Mean Absolute Error E_A

$$E_A^{(j)} = \frac{1}{M}\sum_{i=1}^{M}\left|V_R^{(i,j)} - V_C^{(i,j)}\right|$$

- Root Mean Squared Error $\boldsymbol{E_R}$

$$E_R^{(j)} = \frac{1}{M}\sqrt{\sum_{i=1}^{M}\left[V_R^{(i,j)} - V_C^{(i,j)}\right]^2}$$

- Mean Percent Absolute Error $E_{\%}$

$$E_{\%}^{(j)} = 100\,\frac{1}{R^{(j)}\cdot M}\sum_{i=1}^{M}\left|V_R^{(i,j)} - V_C^{(i,j)}\right|$$

where $R^{(j)}$ is the range in which the variable j^{th} is defined.

- Standard deviation of errors σ_E

$$\sigma_E^{(j)} = \frac{1}{M}\sqrt{\sum_{i=1}^{M}\left[E^{(i,j)} - \overline{E}^{(j)}\right]^2}$$

where $E^{(i,j)}$ is the i^{th} error of the j^{th} variable, while $\overline{E}^{(j)}$ is the mean value of the j^{th} variable.

- Index of agreement $\boldsymbol{d}$

$$d^{(j)} = 1 - \frac{\sum_{i=1}^{M}\left[V_R^{(i,j)} - V_C^{(i,j)}\right]^2}{\sum_{i=1}^{M}\left[\left|V_R^{(i,j)} - \overline{V}_C^{(j)}\right| + \left|V_C^{(i,j)} - \overline{V}_R^{(j)}\right|\right]^2}$$

where $\overline{V}_C^{(j)}$ and $\overline{V}_R^{(j)}$ are, respectively, the mean values of the j^{th} calculated variable and the j^{th} real one.

Numerical Results

The values obtained for the considered performance indexes, referring to the inversion of about 300 models, that where chosen in order to represent the whole space of parameters, are reported in the following Tab. II

Parameter	E_M	E_A	E_R	$E_{\%}$	σ_E	d
σ	3.421	17.0	22.874	4.736	22.616	0.987
δ	0.75	4.4	5.867	4.937	5.818	0.987
L	66.21	359.5	452.358	5.993	447.486	0.982
W	32.98	279.9	345.664	6.999	344.087	0.977
U3	0.047	0.28	0.355	7.223	0.352	0.975
Xb	-35.4	245.13	331.324	2.451	329.419	0.997
Yb	-29.1	224.82	297.090	2.248	295.654	0.997
Zb	28.0	378.3	470.535	6.307	469.701	0.981

Table II Performance indexes.

It can be seen that all the model parameter are estimated with an average error E% that is lower that 10% in case of free-noise data. In more detail the source coordinates Xa and Xb are obtained with lower that 3% while for Zb the average error reaches 7%. The L, W and U3 parameters are estimated with E% around 7% while the Strike and Deep angles are both estimated with E% of about 5%. Moreover, it has been estimated that when the test data are corrupted with a gaussian type noise up to 30% the coordinates Xa and Xb are obtained with $E_{\%}$ lower that 5% while for Zb, L and W the average error reaches about 10%. Finally the Strike and Deep angles are both estimated with $E_{\%}$ of about 15%

Conclusions

This paper has proposed a method for the nonlinear inversion SAR interferometric data by using a SA optimisation algorithm. More specifically, it has dealt with the inversion of ground deformation data relating to magma-filled dikes in volcanic areas. Situations of this kind are very frequent in areas like that of Mt. Etna. To guarantee a sufficient set of data for the study, the data was synthesised using models proposed by Okada. The results presented are essentially as follows. It was first experimentally demonstrated that the inversion procedure using SA can be unambiguously solved. As regards the degree of accuracy, the results obtained confirm the reliability of SA in determining the most important parameters of the model, i.e., the source coordinates and orientation, even in the presence of noise-affected data.

Acknowledgements

This work was supported by the Italian GNV (Gruppo Nazionale per la Vulcanologia) under the coordinate project " Development and application of Remote sensing methods for the monitoring of active italian volcanoes".

References

Briole, P., Avallone, A.,Beauducel, F., Bonforte, A., Cayol, V., Deplus, C., Delacourt, C., Froger, J. L., Malengreau, B., Puglisi, G., (1999). *Interferometrie Radar Appliquée aux Volcans: Cas de L'Etna et des Champs Phlégréens (Italie)*. Rapport Quadriennal CNFGG 1995-1998, pres. at Union Internationale de Geodesie et Geophysique, Birmingham, 121-128.

Coltelli, M., Dutra, L., Fornaro, G., Franceschetti, G., Lanari, R., Migliaccio, M., Moreira, J. R., Papathanassiou, K. P., Puglisi, G., Riccio, D., Schwäbisch, M., (1996). *SIR-C/X-SAR Interferometry over Mt. Etna: DEM Generation, Accuracy Assessment and Data Interpretation.* DLR-Forschungsbericht 95-48.

Curlander, J. C. and McDonough, R. N., (1991). *Synthetic Aperture Radar, Systems & Signal Processing*, Introduction to SAR (J. J. Wiley & Sons Inc, New York.

Gabriel, A. K., Goldstein, R. M., Zebker, H. A., (1989*). Mapping Small Elevation Changes over Large Areas: Differential Radar Interferometry*. Journal of Geophysical Research 94, B7 9183-9191.

Lanari, R., Fornaro, G., Riccio, D., Migliaccio, M., Papathanassiou, K. P., Moreira, J. R., Schwäbisch, M., Dutra, L., Puglisi, G., Franceschetti, G., Coltelli, M., (1996). *Generation of Digital Elevation Models by Using SIR-C/X-SAR Multifrequency Two-Pass Interferometry: The Etna Case Study*, IEEE Trans. on Geoscience and Remote Sensing, 34, 5 1097-1114.

Massonnet, D. and Rabaute, T., (1993). *Radar Interferometry: Limits and Potential*. IEEE Trans. on Geoscience and Remote Sensing, 31, 2 435-464.

McCloy, K. R., (1995). *The physical principles of remote sensing, Resource Management Information System – Process and Practice*. Taylor & Francis press, chp 2 , 67-96

Okada, Y, (1985). *Surface deformation due to shear and tensile faults in a halfspace*. Bull. Seismol. Soc. Amer., vol. 75, pp. 1135–1154.

Scherbaum, F., Palme, C., Langer, H. (1994). *Model Parameter Optimization for Site Dependent Simulation of Ground Motion by Simulated Annealing: Reevaluation of the Ashigara Valley Prediction Experiment*. Nat. Hazards, 10, pp. 275-296.

Sen, M.K. and Stoffa, P. L., (1991). *Nonlinear One-Dimensional Seismic Waveform Inversion Using Simulated Annealing.* Geophysics 1624-1638.